*International Journal of Microwave and Wireless Technologies*, 2017, 9(8), 1597–1602. 
doi:10.1017/S1759078717000897

RESEARCH PAPER

# ANN-based radar approach to detect breast cancers in fibro-glandular tissues: numerical analysis

SALVATORE CAORSI AND CLAUDIO LENZI

*This paper presents a new artificial neural network (ANN)-based radar data processing approach for the detection of breast cancers located inside fibro-glandular tissues. The aim is not the breast imaging but detecting tumors through ANN processing of data extracted from the radar signals measured around the breast. The proposed approach has been assessed using several realistic two-dimensional breast geometries derived from the models provided by the numerical breast phantom repository of the University of Wisconsin Cross-Disciplinary Electromagnetic Laboratory (UWCEM). The pulsed radar system was assumed to operate in the mono-static configuration. The obtained results showed the abilities of the proposed approach to detect, for any single radar trace, tumors located inside the fibro-glandular tissues with a sensitivity of 93%, a specificity of 90%, and an overall accuracy of 92%.*

**Keywords:** Breast cancer detection, Inverse scattering, Artificial neural network

Received 20 December 2016; Revised 17 July 2017; Accepted 24 July 2017; first published online 22 August 2017

## I. INTRODUCTION

According to recent statistical reports of the American Cancer Society [1], breast cancer is the most diffused topology of tumor among females. Currently, the X-ray mammogram represents the standard diagnostic technique. Nevertheless, it is well known that it presents several problems and limitations. Mainly its ionising radiation can lead to further develop tumors. In addition, especially in dense breast, the X-ray mammogram suffers from low and unstable values of sensitivity, varying from 66 to 96% [2]. In order to improve the performance, the X-ray mammogram can be used in conjunction with other diagnostic techniques, such as magnetic resonance imaging, ultrasound, and the simple clinical examination. However, clinical studies have found that although their combined use can improve the value of sensitivity or specificity, the overall accuracy varies from 66.6 to 75.6% [2].

During last decades, in order to overcome mammograms' limitations, new detection techniques have been proposed. Among these, the differences in electromagnetic properties at microwave frequencies between malignant and healthy breast tissues [3], have motivated the development of the microwave imaging techniques. Microwave tomography [4, 5] and ultra-wide band (UWB) radar imaging techniques [6, 7] are the most promising active approaches proposed in the literature.

Department of Electrical, Computer and Biomedical Engineering, University of Pavia, via Ferrata 5, 27100 Pavia, Italy
**Corresponding author:**
C. Lenzi
Email: claudio.lenzio1@ateneopv.it

In this paper, extending the results of our previous work on subcutaneous breast tumors [8], we aim to evaluate a new artificial neural network (ANN)-based radar data processing approach to diagnose tumors deep seated inside fibro-glandular tissues.

For each radar trace recorded around the breast, our purpose is to detect the presence of a cancer independently of its depth and width. To this end, the primary step is extracting, from the radar signals, the data that best detect the tumor's presence. Then an ANN architecture is designed for optimal processing of the extracted radar data. The proposed approach is able to provide several advantages including a significant reduction of the computational burdens, with the possibility of reaching quasi-real-time responses.

## II. THE ANN-BASED RADAR APPROACH MATERIALS AND METHOD

The present work considers two-dimensional (2D) breast geometries and a pulsed mono-static radar system that moves along an axial circular line around the body and gives, for each angular position, the radar trace in the time domain. According with such a problem geometry, the backscattered radar signals were simulated using the finite-difference time-domain-based software GprMax [9]. The transmitting mono-static radar antenna was modeled using an elementary Hertzian dipole. The receiving mono-static radar antenna was ideally and numerically simulated as a space point in which the electromagnetic field is measured. For each angular

position, the transmitting and receiving antennas coincide in the same space point.

Each single radar trace is then processed by an ANN to reveal, trace by trace, the presence of a tumor located inside fibro-glandular breast tissues. To do this, the ANN needs to be trained with data extracted from the radar signal. The idea is to exploit the information contained in the amplitudes ($A_1$, … $A_i$, … $A_N$) and the times of arrival ($t_1$, … $t_i$, … $t_N$) of $N$ suitable local maxima and minima. In order to deduce what and how many local peaks should be chosen, a preliminary assessment study of the signals will be performed in Section III.

The ANN architecture used consists of a multilayer, feed-forward, fully connected network [10]. As represented in Fig. 1, this type of ANN is formed by an input layer, one or more hidden layers, and one output layer. Each layer is formed by a fixed number of nodes that represent the artificial neurons, and each node is connected to every one of the adjacent layers. To each connection – between the generic node $j$ of the layer $k$ and the generic node $i$ of the previous layer $(k-1)$ – is associated a constant $w_{ij}^{k-1,k}$ that represents the weight of the connection. Moreover, to each artificial neuron $j$ is associated a term of bias $w_{oj}^{k}$.

The ANN is trained using a set of input–output pairs, the so-called "examples," and their number is strictly related to the number of weights and bias. During this forming phase, through a minimization process, for all the input–output pairs, the ANN iteratively adjusts the weights and bias with the aim of minimizing the errors between the desired output values and those effectively reconstructed by the network [10].

Once the training phase is completed, all the weights and biases are stored, and the network is ready to be used in the next phases of test and "on-field" operating mode. Even if the network training phase is time consuming and carries a high computational burden, it does not represent a problem because it is an "off-line" phase. Instead during both the test and "on-field" phases, the network provides results in quasi-real time and with a very low computational burden. Indeed, the use of ANNs allows one to reformulate the inverse scattering problem by considering only a lower set of unknowns describing the object to be detected.

The number of nodes of the input and the hidden layers will be discussed in the following sections. Instead, it is worth noting that, for the purposes of the present diagnostic method, ANN architectures – having as the output layer only a single node – will be considered. This choice was made in order to provide an output of type yes/no, depending on the presence (yes) or absence (no) of tumors.

In our previous work [8], we obtained interesting results for subcutaneous tumors using UWB pulses with a central frequency of 2 GHz and a time duration of 1 ns. However, other works [11, 12] have instead used central frequencies of about 6 GHz with a time duration 0.3 ns for breast imaging purposes. For these reasons in the present paper, we wanted to assess these two different radiating pulses. As shown in Fig. 2, for each frequency, we used a differentiated Gaussian pulse as a signal waveform to produce a higher power of the backscattered signal [13]. For this reason, it is more suitable in detecting targets that are deeply located [13].

To characterize the healthy tissues in the 2D geometries used, we considered the Debye equation where the suitable values for the static relative permittivity ($\varepsilon_s$), the relative permittivity at infinite frequency ($\varepsilon_\infty$), the conductivity ($\sigma$), and the relaxation time ($\tau$) have been taken by [14].

The tumor was modeled by placing a circular dielectric anomaly inside the fibro-glandular tissue area. The values for the Debye dielectric parameters ($\varepsilon_s$, $\varepsilon_\infty$, $\sigma$, and $\tau$) were obtained starting from the Cole–Cole representation provided in [15] and minimizing the cost function reported by [16].

## III. IDEAL BREAST MODELS

Preliminarily, the ideal cases of different cancerous breasts, consisting of 2D homogeneous and concentric three-layered geometries, have been studied.

In particular, we considered the following three healthy tissues: the skin, the adipose tissue, and the fibro-glandular tissue. Each tissue was dielectrically characterized using the Debye model and the tumor placed inside the fibro-glandular tissue area was characterized by means of the Debye dielectric parameters ($\varepsilon_s$, $\varepsilon_\infty$, $\sigma$, and $\tau$) as was already described in the previous section.

As can be expected, for such ideal cases, the presence of the anomaly can be detected by simply inspecting all the radar traces recorded around the breast geometry or, in a more effective way, by simply inspecting the radar grams. The representation through the radar gram is commonly used to visualize radar signals in ground-penetrating radar applications [9]. For our purposes, it consists of an image that represents all the radar signals measured around the breast placed adjacent one to the other. In such a way the horizontal axis

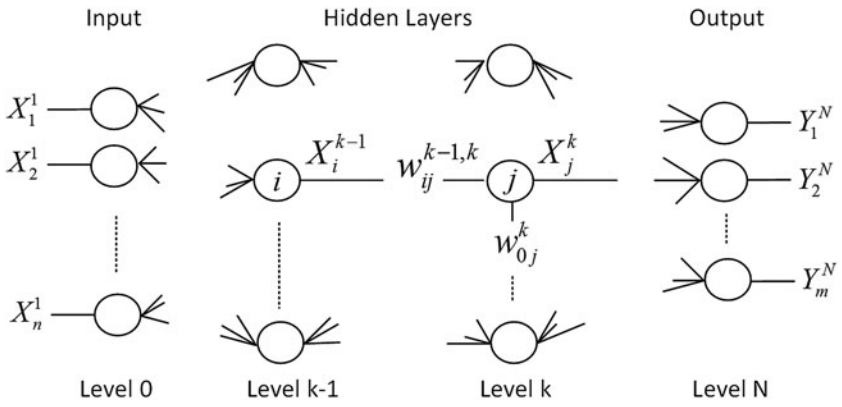


**Fig. 1.** Schematic representation of an ANN architecture of the multilayer, feed-forward, and fully connected type.

https://doi.org/10.1017/S1759078717000897 Published online by Cambridge University Press

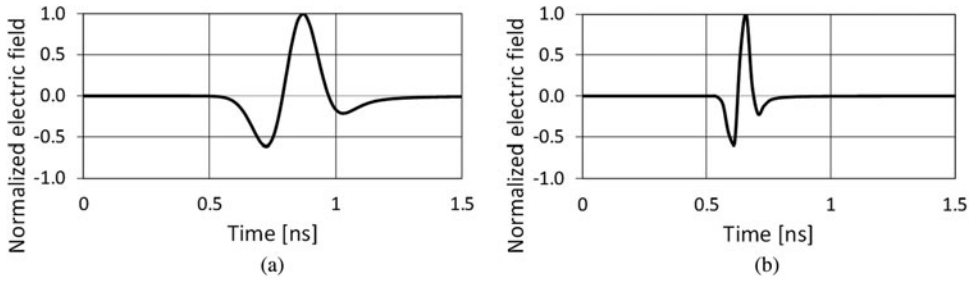


**Fig. 2.** The UWB differentiated Gaussian pulses: (a) UWB pulse with central frequency 2 GHz and time duration 1 ns; (b) central frequency 6 GHz and time duration 0.3 ns.

represents the radar angular position, whereas the vertical axis is the time evolution of each recorded signal.

Nevertheless, as it is proved in the literature [7, 11, 12, 17–21], the dynamic between the tumor's signature and the echoes backscattered from the skin is very high. Moreover, in some cases, such echoes can also overlap and mask the searched tumor presence. In the literature, several cleaning techniques were proposed in order to suppress the strong components backscattered from the skin [7, 11, 12, 17–21]. Among these, a skin's reflection reduction particularly useful for ANN-based radar detection approaches has already been studied in our previous work [21]. However, in the present paper, because we are aiming to perform a preliminary numerical assessment, we applied an ideal cleaning technique. For each angular position of the mono-static radar antenna, the ideally cleaned signal is obtained by subtracting from the total backscattered signal the radar signal measured on the same radar position, but on a reference two-layered cleaning model composed only of skin and adipose tissue. In this way, the signal components due to the presence of the skin are strongly reduced, whereas the contributions due to the presence of the fibro-glandular tissue and the tumor signature are evident.

In this context, we analyzed the radar traces simulated on 30 different cancerous biological models. These were obtained by sweeping the dimensions of the entire 2D three-layered geometry, the dimensions of both the adipose and fibro-glandular layers, and the tumor diameters and by positioning the tumor at different depths inside the fibro-glandular tissue. The obtained results can be summarized by looking at the radar grams reported in Fig. 3 and obtained in the case where the incident UWB pulse with central frequency of 2 GHz is used.

In particular, Fig. 3 shows the radar grams of the ideally cleaned radar signals measured on an ideal breast geometry in which a dielectric anomaly has been inserted at two different depths inside the fibro-glandular tissue. The radius of the breast geometry was 8 cm, the skin thickness was 1.5 mm, and the radius of the fibro-glandular tissue was 6 cm. Figures 3(a) and 3(b) show the cases where the dielectric anomaly of 6 mm in diameter is positioned 0.4 and 3.6 cm, respectively, inside the fibro-glandular tissue.

For such cases, because the radar signal has been cleaned by the air–skin reflections, the first reflected echoes are associated to the fat/fibro-glandular interface. Due to the circular 2D geometry, the distance of the radar from the fibro-glandular layer is constant. For this reason, in Fig. 3 the first straight lines between 1.2 and 2.2 ns are given by the reflections of the fibro-glandular layer. Instead, because the distance between the radar and the tumor changes when the radar moves in a circle around the geometry, the presence of the tumor is identified by a curved line. In particular, Fig. 3(a) shows that when the tumor is positioned closer to the outer surface of the fibro-glandular tissue, its signature is partially overlapped with the signals backscattered from the interface between the adipose and fibro-glandular tissue. In contrast, Fig. 3(b) shows that, if the tumor is located deep inside the fibro-glandular tissue, its signature is completely visible. It is worth noting that, for both the cases, the tumor signature is contained in the second part of the ideally cleaned radar signal.

On the basis of the analyses conducted and of the discussion noted earlier, we concluded that if we want to find suitable information in order to characterize the presence of tumors located inside the fibro-glandular tissue, these data must be searched inside the second part of the cleaned radar signals. According to the earlier conclusions, starting from the ideally cleaned radar signals obtained in both the cases where the UWB pulses at 2 and 6 GHz are used, we exploited the information that is contained in the amplitudes and arrival times of the third, fourth, and fifth local maximum/minimum of such signals.

Using these data, we trained and tested different ANN architectures receiving different input data and providing a

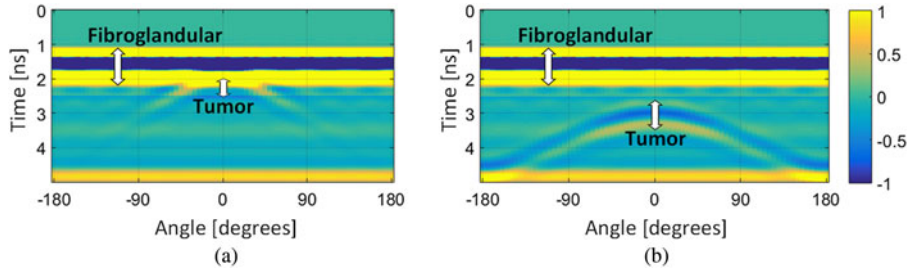


**Fig. 3.** The radar grams of the ideally cleaned radar signals. (a) Dielectric anomaly located close to the outer surface of the fibro-glandular tissue; (b) anomaly positioned deep inside the fibro-glandular tissue.

https://doi.org/10.1017/S1759078717000897 Published online by Cambridge University Press

binary output, of type yes/no, in order to discriminate the tumor presence. In particular, three different ANNs have been considered: the ANN 6-12-1 that works on the amplitudes and arrival times of the third, fourth, and fifth local maxima/minima; two different ANNs of type 4-8-1 working, respectively, on the amplitudes and arrival times of the third and fourth peaks and of the fourth and fifth maxima/minima. It means that the ANN 6-12-1 and the ANNs 4-8-1 have, respectively, six and four input nodes, and only one output node (yes/no). According to our previous experiences [8], we chose to use for all three ANNs only one hidden layer, with a number of nodes equal to double of that of the input layer.

The results obtained with all three ANN architectures applied to 2D ideal breast models have provided excellent results for both frequencies of the UWB radar pulses used, reaching values of sensitivity, specificity, and accuracy that never fell below 98%.

## IV. REALISTIC BREAST MODELS

Because the ideal case of homogeneous 2D geometries presented in Section III obtained, as expected, excellent results, we also assessed the capabilities of our approach in the case of realistic 2D breast models derived by the University of Wisconsin Cross-Disciplinary Electromagnetic Laboratory (UWCEM) database [14].

Starting from the nine 3D breast models provided by the UWCEM database, we built several realistic 2D cancerous and healthy breast geometries. The healthy breast geometries were built by randomly choosing the model, the section, and the Debye parameters ($\varepsilon_s$, $\varepsilon_\infty$, $\sigma$, and $\tau$) for the dielectric characterization of the tissues. These values were chosen in the same range of values already cited in Section II. Each obtained geometry allows us to discriminate eight different typologies of healthy breast tissue: the skin, three typologies of adipose tissue, a transitional tissue, and three different typologies of fibro-glandular tissue. Each cancerous geometry was built starting from a new healthy geometry in which a circular dielectric anomaly has been inserted inside the fibro-glandular tissues. The dielectric anomalies were randomly generated by randomly choosing both the diameter value (between 0.2 and 1 cm) and the locating depth. The values for the Debye dielectric parameters ($\varepsilon_s$, $\varepsilon_\infty$, $\sigma$, and $\tau$) were obtained in the same way already described in Section II. An example of the cancerous geometries used is reported in Fig. 4.

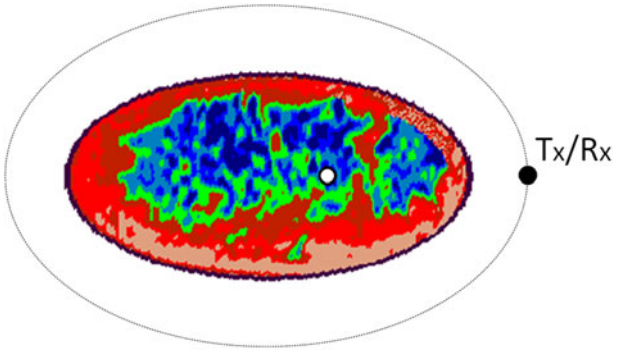


**Fig. 4.** A realistic 2D cancerous geometry with a tumor located inside the fibro-glandular tissues.

As discussed in Section III, in order to suppress the strong skin reflections, we applied an ideal cleaning technique where, for each angular radar position, the ideally cleaned radar signal was obtained by subtracting from the total one the signal measured on the same 2D geometry, but formed by only the skin and adipose tissue. Moreover, because in the realistic geometries the distance between the radar antenna and the breast surface is no longer constant, the times of arrival and the amplitudes of the measured backscattered signals change between different radar positions. In order to reduce this space-temporal error, we applied a cross-correlation technique in order to measure the arrival time of the total backscattered signal, then the resulting arrival times were used as zero reference times for all the recorded radar signals. At last, the amplitude of the signal has been multiplied by a coefficient that takes into account the temporal shift [22].

Following the promising results obtained in the cases of ideal breast models, in order to best characterize the presence of the tumor, we searched for suitable information inside the second part of the cleaned and equalized radar signals obtained by using both the UWB pulses with central frequencies of 2 and 6 GHz.

At this point, different ANN architectures working with different data inputs and providing a binary output, of type yes/no, were trained and tested. In particular, we trained an ANN of type 6-12-1 that works on the amplitudes and arrival times of the third, fourth, and fifth maxima/minima. Moreover, an architecture of type 4-8-1 has been designed for working, respectively, on the amplitudes and arrival times of the third and fourth peaks, and on the data of the fourth and fifth peaks. All the networks have been trained and tested by using the two different incident pulses.

According to the number of degrees of freedom, each network has been trained using a fixed number of training data. In particular, the architectures of type 4-8-1 have been trained using 100 training examples, namely 50 measured on cancerous geometries (T) and 50 measured on healthy breast models (NT); however, during the training process of the networks 6-12-1, a set of 200 input–output pairs, consisting of 100 T geometries and 100 NT geometries, was used. The results obtained during the training phases were highly satisfactory, providing values of accuracy equal to 100%. These results show that, for both the incident pulses, all the networks have been able to adjust both the weights and bias of their internal nodes in order to find the best connections between the input–output pairs furnished during the training process.

In order to test the networks in a significant and general way, we simulated the radar signals measured on new healthy and malignant breast geometries. In this way, all the networks were validated using 60 new geometries, namely 30 T and 30 NT. The results were highly satisfactory, and they are reported in Tables 1 and 2.

**Table 1.** Performance on testing data – 2 GHz.

| ANN architecture | ANN performance (%) | | |
|---|---|---|---|
| | Sensitivity | Specificity | Overall accuracy |
| 4-8-1 (third, fourth peak) | 93 | 90 | 92 |
| 4-8-1 ( fourth, fifth peak) | 70 | 73 | 72 |
| 6-12-1 (third, fourth, fifth peak) | 80 | 77 | 78 |

https://doi.org/10.1017/S1759078717000897 Published online by Cambridge University Press

**Table 2.** Performance on testing data – 6 GHz.

| ANN architecture | ANN performance (%) | | |
|---|---|---|---|
| | Sensitivity | Specificity | Overall accuracy |
| 4-8-1 (third, fourth peak) | 90 | 87 | 88 |
| 4-8-1 ( fourth, fifth peak) | 67 | 73 | 70 |
| 6-12-1 (third, fourth, fifth peak) | 77 | 73 | 75 |

In particular, Table 1 reports the results obtained using the UWB pulse at 2 GHz, and Table 2 shows the results obtained where the pulse at 6 GHz is used. Looking at the tables it is evident that, despite the fact that all the networks have detected the presence of the tumor with values of accuracy >70%, the best results were obtained by using the ANN architecture of type 4-8-1 that works on the third and fourth maxima/minima of the ideally cleaned radar signals – namely the ANN 4-8-1 (third and fourth peaks). Indeed, in the case where the UWB pulse at 2 GHz is used, Table 1 shows that the tumor was detected with a sensitivity of 93% (corresponding to a false-negative ratio of 7%), a specificity of 90% (namely a false-positive ratio of 10%), and an overall accuracy equals to 92%. Looking at Table 2, in the case where the UWB pulse at 6 GHz is used, the tumor was detected with a sensitivity of 90% (false-negative ratio of 10%), a specificity of 87% (false-positive ratio of 13%), and an overall accuracy of 88%.

## V. CONCLUSION

In this paper, we proposed and tested a new ANN-based radar data processing approach for detecting breast tumors located inside fibro-glandular tissues. Using a mono-static radar system, the backscattered signals are measured around the breast, then suitable data are extracted and ANN processed in order to detect the presence of internal tumors.

In order to preliminarily assess the proposed approach, several 2D homogeneous three-layered cancerous geometries were studied in the case where an ideal skin-artifact removal technique is applied. The results showed that for such cases, the tumor can be detected by simply inspecting the radar grams of the radar signals measured around the breast geometry. Moreover, using different ANNs working on the second part of such signals, namely the third, fourth, and fifth local maxima/minima of the cleaned radar signals, the achieved values of sensitivity, specificity, and accuracy were >98%.

On the basis of these expected excellent preliminary results, we considered 2D realistic cancerous and healthy breast models derived from the models of the UWCEM database. In this way, several new ANNs were trained and tested exploiting, like in the previous homogeneous cases, the information contained in the second part of the ideally cleaned radar signals. The best results were obtained by using the ANN 4-8-1 that works on the amplitudes and arrival times of the third and fourth maxima/minima of the cleaned radar signals. In the case where the UWB pulse with central frequency of 2 GHz is used as the illuminating signal, the presence of the tumor was detected with a sensitivity of 93%, a specificity of 90%, and an overall accuracy of 92%. However, in the case where the UWB pulse with a central frequency of 6 GHz is used, the tumor has been detected with a sensitivity of 90%, a specificity of 87%, and an overall accuracy of 88%.

The encouraging results motivate us to move forward on this topic, studying the performance in the cases where the proposed technique is applied to more realistic scenarios. First of all, attention will be focused on removing the strong skin reflections using a realistic cleaning technique. As mentioned in Section III, several cleaning methods were proposed in the literature [7, 11, 12, 17–21]. As first step, we will apply the realistic model-based cleaning technique designed in our previous work [21]. Moreover the proposed technique needs to be studied and assessed using 3D realistic breast models.

## ACKNOWLEDGEMENTS

All the data and information used in the present work are listed in the references, figures, and tables.

## REFERENCES

[1] American Cancer Society, Cancer Facts & Figures 2015, Atlanta, GA, USA, American Cancer Society, 2015.

[2] Hassan, A.M.; El-Shenawee, M.: Review of electromagnetic techniques for breast cancer detection. IEEE Rev. Biomed. Eng., **4** (2011), 103–118.

[3] Hagness, S.C.; Taflove, A.; Bridges, J.E.: Two-dimensional FDTD analysis of a pulsed microwave confocal system for breast cancer detection: fixed-focus and antenna-array sensors. IEEE Trans. Biomed. Eng., **45** (1998), 1470–1479.

[4] Shea, J.D.; Van Veen, B.D.; Hagness, S.C.: A TSVD analysis of microwave inverse scattering for breast imaging. IEEE Trans. Biomed. Eng., **59** (2011), 936–945.

[5] Fang, Q.; Meaney, P.M.; Paulsen, K.D.: Viable three-dimensional medical microwave tomography: theory and numerical experiments. IEEE Trans. Antennas Propag., **58** (2010), 449–458.

[6] Fear, E.C.; Li, X.; Hagness, S.C.; Stuchly, M.A.: Confocal microwave imaging for breast cancer detection: localization of tumors in three dimensions. IEEE Trans. Biomed. Eng., **49** (2002), 812–822.

[7] Yin, T.; Ali, F.H.; Reyes-Aldasoro, C.C.: A robust and artifact resistant algorithm of ultrawideband imaging system for breast cancer detection. IEEE Trans. Biomed. Eng., **62** (2015), 1514–1525.

[8] Caorsi, S.; Lenzi, C.: Can an ANN based radar data processing approach be an aid in breast cancer detection?, in IEEE Int. Conf. on Electromagnetics in Advanced Applications (ICEAA), Turin, Italy, 2015.

[9] Giannopoulos, A.: Modelling ground penetrating radar by GprMax. Constr. Build. Mater., **19** (2005), 755–762.

[10] Haykin, S.: Neural Networks: A Comprehensive Foundation. Prentice-Hall, New York, NY, USA, 1994.

[11] Li, X.; Hagness, S.C.: A confocal microwave imaging algorithm for breast cancer detection. IEEE Microw. Wireless Compon. Lett., **11** (2001), 130–132.

[12] Zhi, W.; Chin, F.: Entropy-based time window for artifact removal in UWB imaging of breast cancer detection. IEEE Signal Process. Lett., **13** (2006), 585–588.

[13] Uduwawala, D.: Gaussian vs differentiated gaussian as the input pulse for ground penetrating radar applications, in Int. Conf. on

https://doi.org/10.1017/S1759078717000897 Published online by Cambridge University Press

Industrial and Information Systems (ICIIS), Penadeniya, Sri Lanka, 2007.

[14] Zastrow, E.; Davis, S.K.; Lazebnik, M.; Kelcz, F.; Van Veem, B.D.; Hagness, S.C.: Database of 3D Grid-Based Numerical Breast Phantoms for use in Computational Electromagnetics Simulations, Department of Electrical and Computer Engineering University of Wisconsin-Madison. http://uwcem.ece.wisc.edu/MRIdatabase/InstructionManual.pdf.

[15] Lazebnik, M.; Popovic, D.; McCartney, L.; Watkins, C.B.; Lindstrom, M.J.; Harter, J. et al.: A large-scale study of the ultrawideband microwave dielectric properties of normal, benign, and malignant breast tissues obtained from cancer surgeries. Phys. Med. Biol., **52** (2007), 6093–6115.

[16] Lazebnik, M.; Okoniewski, M.; Booske, J.H.; Hagness, S.C.: Highly accurate Debye models for normal and malignant breast tissue dielectric properties at microwave frequencies. IEEE Microw. Wireless Compon. Lett., **17** (2007), 822–824.

[17] Maskooki, A.; Gunawan, E.; Soh, S.B.; Low, K.S.: Frequency domain skin artifact removal method for ultra-wideband breast cancer detection. Prog. Electromagn. Res., **98** (2009), 299–314.

[18] Maklad, B.; Fear, E.C.: Reduction of skin reflections in radar-based microwave breast imaging, in IEEE Int. Conf. of the Engineering in Medicine and Biology Society (EMBS), Vancouver, BC, 2008.

[19] Klemm, M.; Craddock, I.J.; Leendertz, J.A.; Preece, A.; Benjamin, R.: Improved delay-and-sum beamforming algorithm for breast cancer detection. Int. J. Antennas Propag., **2008** (2008), 1–9.

[20] Bond, E.J.; Li, X.; Hagness, S.C.; Van Veen, B.D.: Microwave imaging via space-time beamforming for early detection of breast cancer. IEEE Trans. Antennas Propag., **51** (2003), 1690–1705.

[21] Caorsi, S.; Lenzi, C.: Skin artifact removal technique for breast cancer radar detection. Radio Sci., **51** (2016), 767–778.

[22] Richards, M.A.; Scheer, J.A.; Holm, W.A.: Principles of modern radar. SciTech Pub, Raleigh, NC, 2010.

**Salvatore Caorsi** is a full Professor of Electromagnetic Compatibility at the University of Pavia where he is teaching Electromagnetic Compatibility, Electromagnetic Inverse Scattering and Diagnostic, Electromagnetic Field and Environmental Impact. His primary activities are focused on the evaluation of electromagnetic fields in complex domain, non-linear scattering, electromagnetic compatibility, inverse scattering mainly devoted to electromagnetic techniques for remote sensing and diagnostics, and electromagnetic application in biomedical field. He founded in 1990 a National Research Center on the Interaction between Electromagnetic Field and Biosystems (ICEmB) for which he is now serving as Director. He has been the chairman for many research units in national and international research projects and the organizer of scientific sessions and workshop in the context of national and international congress and symposia. He is the author of more than 250 papers published in scientific journals, conference proceedings, and summaries.

**Claudio Lenzi** received the Ph.D. in Electronics, Computer Science, and Electrical Engineering from the University of Pavia in 2017. At present, he is a postdoctoral researcher at the Microwave Laboratory of the University of Pavia. His research activity is mainly focused on numerical modeling, machine learning, and the analysis and processing of radar signals and data for biomedical engineering applications.

https://doi.org/10.1017/S1759078717000897 Published online by Cambridge University Press